

EXPLORING THE USE OF IN-HOUSE SODIUM SILICATE FROM AGRO-INDUSTRIAL BY-PRODUCTS IN PERVIOUS GEOPOLYMER CONCRETE

Robberta Renuka LAZARUS¹, U. JOHNSON ALENGARAM^{1✉},
 Wan Zurina WAN JAAFAR¹, Sai Hin LAI²,
 Muhammad Shazril Idris Bin IBRAHIM¹, Karthick SRINIVAS M¹

¹Centre for Innovative Construction Technology (CTCT), Department of Civil Engineering,
 Faculty of Engineering, Universiti Malaya, 50603 Kuala Lumpur, Malaysia

²Department of Civil Engineering, Faculty of Engineering, University Malaysia Sarawak, 94300,
 Kota Samarahan, Sarawak, Malaysia

Article History:

- received 1 September 2024
- accepted 20 January 2025

Abstract. The extraction of in-house sodium silicate (IHS) as an alternative to commercial silicate in geopolymer pervious concrete (GPC) is the focus of this research. The IHS was developed from rice husk ash (RHA) and treated palm oil fuel ash (TPOFA) using the hydrothermal method. Class F Fly Ash (FA) and Ground Granulated Blast Furnace Slag (GGBS) were used as precursors in a 70:30 ratio. Steel slag aggregate (SSA) was used to wholly replace the conventional aggregates. Palm kernel shell biochar (PKS-BC) at various weight percentages between 1 and 5% was used to replace coarse aggregates (CA). GPC specimens were prepared using 10 M sodium hydroxide (NaOH) and one of the SS: commercial SS, RHA-based IHS, and a 'Hybrid SS' (commercial SS: TPOFA-based IHS – 50:50). The findings revealed that due to the toughness, surface roughness, and shape of the SSA, the compressive strength of SSA-based GPC specimens produced higher strength compared to crushed granite aggregate (CGA)-based GPC. 'Hybrid SS' and RHA-based IHS yielded slightly higher compressive strengths in GPC specimens compared to commercial SS-based GPC specimens. This finding proved that the appropriate ratio of silica source with NaOH facilitates the development of SS in the development of GPC.

Keywords: geopolymer pervious concrete, in-house sodium silicate, hydrothermal method, palm kernel shell biochar, UV spectrophotometer.

✉Corresponding author. E-mail: johnson@um.edu.my

1. Introduction

As well documented, concrete is a widely used material due to its versatile nature, and currently 25 billion tons of concrete are generated globally on a yearly scale (Wang et al., 2018). The demand for concrete is increasing as the need for shelter and construction is rising due to globalization and industrialization (Nurruddin et al., 2018). One significant observation of using huge quantities of cement and concrete is the reduction of porous soil that allows water percolation to increase the water table. This scenario is detrimental as soil surfaces are rapidly cemented, causing dire issues like flooding, and stormwater runoffs. For instance, in late 2014, a flooding issue in Malaysia affected 500,000 victims and led to a loss worth RM2.85 billion (Wahid et al., 2018). In addition, the increased urbanization leads to reduced infiltration, reduced ground-water recharge, and degraded water environment quality

(Liu et al., 2020). On the other hand, black-bodied asphalt concrete which possesses low albedo and high heat capacity is commonly used in the pavement system, resulting in Urban Heat Island (UHI) effect (Mohajerani et al., 2017). These scenarios prove the need for significant measures to address the dire problems without jeopardizing the environment.

Researchers are actively searching for green and cost-effective methods to address such issues and pervious pavement is found to be an efficient measure in addressing environmental problems considering the factor 'sustainability' according to Soundararajan and Vaiyapuri (2021). Pervious concrete (PC) is deemed the best of all types of permeable pavement, as it recharges ground-water (Srikanth & Dakshina Murthy, 2021; Soundararajan & Vaiyapuri, 2021). PC has various terms such as porous,

permeable, pervious, no-fines concrete, self-draining, or 'thirsty concrete' (Jadhav et al., 2022). Since the middle of the 19th century, PC has been used in building construction due to its ability to address stormwater runoffs, UHI effects, transportation-related noises, and more (da Costa et al., 2021; Cai et al., 2022). From the 1980s onwards, PC has been implemented in various settings such as pedestrian walkways, parking areas, and low-traffic density lanes, as part of experimental and demonstration initiatives in countries like Japan, Europe, Canada, and the United States (Cai et al., 2022; Arun & Chekravarty, 2022). However, existing literature predominantly focuses on cement-based PC, which raise concerns about increased pressure on the limestone resources.

Given that concrete is the second most utilized material globally, following water, it necessitates a substantial quantity of Ordinary Portland Cement (OPC) (Nurrudin et al., 2018). The production of cement involves the calcination of limestone and clay at 1450 °C, followed by the blending of the resulting sintered clinker with limestone and finely ground gypsum (Georgiades et al., 2023). Based on the CO₂ emissions of OPC clinker production from cradle-to-grave, approximately 798 kg (world average) and 712 kg (European average) per ton of clinker is produced which mainly arises from the reactions of raw materials (i.e., process-based) and fossil fuel combustion (i.e., energy-based) (Georgiades et al., 2023). Cement production is estimated at 4.1 billion tons annually (Khan et al., 2020) and accounts for 8% of global greenhouse gas (GHG) emissions. Recent research indicates that the atmospheric concentration of CO₂ is 421 parts per million (ppm), exceeding the clean air standard of 300 ppm, which raises significant environmental concerns (Meskhi et al., 2023).

Few strategies have been suggested in the literature to reduce CO₂ emissions in the production of low-carbon concrete. These strategies include the sequestration of stable carbon within materials without compromising their other properties (Tan et al., 2022), the use of renewable energy in the production processes (Khan et al., 2020), modifications to manufacturing processes, and the partial or complete replacement of OPC with supplementary cementitious materials (SCM) (Khan et al., 2020). It has been demonstrated that SCM can indirectly enhance the mechanical and durability characteristics of concrete (Soundararajan & Vaiyapuri, 2021). Lingyu et al. (2021) found that concrete made with 100% OPC emits 9% more CO₂ compared to geopolymer concrete. Geopolymer concrete, which often incorporates waste materials and industrial by-products, is gaining attention in research (Tan et al., 2020) and is attributed to its technological and operational advantages (Meskhi et al., 2023).

In the context of low-carbon PC fabrication, this study employs industrial and agricultural by-products in the production of geopolymer pervious concrete (GPC). As noted by Thomas et al. (2022), 'geo' refers to geological or industrial materials, while 'polymer' denotes a chain of molecules derived from a common unit. Geopolymer is characterized as environmentally friendly materials featur-

ing three-dimensional silicon-aluminum tetrahedral structures, containing numerous Si-O and Al-O structures (Duxson et al., 2005; Lingyu et al., 2021).

To enhance sustainability by reducing the carbon footprint and utilizing agro-industrial wastes effectively, this study substituted CA with palm kernel shell biochar (PKS-BC) by weight. PKS-BC, a stable pyrolyzed material, has been demonstrated to effectively sequester carbon within its porous and intricate structure. The selection of PKS-BC was motivated by the prevalence of palm-based wastes in Malaysia, the structural stability it offers, and its carbon-negative characteristics.

One of the crucial components of geopolymer concrete involves the utilization of alkaline activators to trigger the precursors. The selected precursors include Class F Fly Ash (FA) and Ground Granulated Blast Furnace Slag (GGBS). The global annual production of FA is estimated to be approximately 750 million tons (Zabihi-Samani et al., 2018). Gupta et al. (2021) mentioned that FA has the potential to reduce CO₂ emissions by 300 million tons per year if 20% of the cement demand is substituted with FA. Conversely, the worldwide production of GGBS is around 530 million tons, with only 65% of it being utilized by the construction industry (Ahmad et al., 2022). GGBS requires 90% less energy for production compared to an equivalent amount of OPC and results in lower CO₂ emissions (Sweeney et al., 2011). Furthermore, GGBS facilitates the formation of calcium silicate hydrate (C-S-H) gel following the initial formation of sodium aluminosilicate hydrate (N-A-S-H) gel, thereby enhancing the mechanical characteristics of concrete (Sachet & Salman, 2021).

The activators in geopolymer concrete commonly consist of sodium or potassium hydroxide and sodium silicates. The production of commercial sodium silicate (SS) involves an energy-intensive process and the utilization of silica-based fine aggregates as the primary material source. The manufacturing process of SS includes the fusion of meticulously selected high-quality silica sand and soda ash at temperatures as high as 1500 °C (Todkar et al., 2016). This process is linked to an emission factor of 1.514 kg CO₂-e per kg of SS (Alnahhal et al., 2023), leading to a substantial carbon footprint. The production of SS from sand or quartz in a furnace is similar to the production of glass and results in silica of inferior purity as depicted by the equation below (Todkar et al., 2016):



The cost of alkaline activators poses a challenge to the widespread adoption of GPC, which could potentially be mitigated by developing an in-house sodium silicate (IHS) using locally available siliceous materials.

This study aimed to develop an IHS using a hydrothermal method, which involves dissolving silica sources at 80 °C. Two silica-based materials, namely rice husk ash (RHA) and treated palm oil fuel ash (TPOFA), were utilized for the extraction of IHS. RHA, an agricultural residue from rice processing mills, is known for its high content of reactive amorphous silica. Rice husk, constituting one-third

of the mass of a rice grain, is a significant crop residue projected to exceed 150 million tons, given that 1 kg of rice milling produces 0.28 kg of rice husk (Siddika et al., 2021). Conversely, TPOFA was chosen due to the significant concern over palm wastes in Malaysia, which is the second-largest palm oil-producing country globally, after Indonesia. Malaysia has over 3.1 million hectares of oil palm trees, resulting in the production of approximately 9 million tons of crude oil. This production process leads to the creation of POFA as a by-product from oil palm shells and oil palm bunches (Tambichik et al., 2018). POFA was further processed for utilization in the form of TPOFA.

The alkaline activator employed in this investigation was a combination of SS and 10M Sodium hydroxide (NaOH). The mixture proportions and stirring durations for the RHA and TPOFA-based IHS are detailed in Table 4, considering the chemical compositions identified through X-Ray Fluorescence (XRF) analysis, as illustrated in Table 3.

The tests conducted on CA included the aggregate impact test (AIT) (British Standards Institution [BSI], 1990), bulk density test (ASTM International, 1997), and specific gravity tests (ASTM International, 2024). The binders underwent laser granulometry test to identify the particle size distribution and FA specifically was confirmed of its pozzolanic property (ASTM International, 2019); the RHA and TPOFA-based IHS were tested for the density, XRF, and viscosity tests. On the other hand, the GPC specimens were tested for compressive strength, porosity test, infiltration test, microstructural analysis, and light reflectivity test.

In this study, a new method for enhancing the strength of GPC specimens, termed 'Hybrid SS', was developed. Hybrid SS involved the mixing of commercial SS and TPOFA-based IHS (50:50 ratio) with 10M NaOH for GPC casting. This approach was adopted as the use of TPOFA-based IHS alone led to the formation of brittle GPC specimens. The potential of Hybrid SS and RHA-based IHS for further enhancement in sustainable geopolymer concrete is highlighted. The study investigates the utilization of unfiltered and ungelated IHS in the casting process, a method that not only reduces waste generation but also cuts costs and enhances the value of agro-industrial by-products.

2. Materials and methods

2.1. Materials

2.1.1. Binders

The binders, class F-FA and GGBS, both obtained from local suppliers, were employed in this research. Figure 1 depicts the particle size distribution of FA and GGBS. FA is a by-product of pulverized coal that is introduced into a fire furnace in a thermal power plant (Patankar et al., 2015) and is rich in alumina oxide (Al_2O_3) and silica oxide (SiO_2) (Kaur et al., 2018). Despite an annual production of around 780 million tons of FA, only a small percentage, ranging from 17 to 20%, is currently being used (Patankar et al., 2015). Class F FA was chosen for its low calcium content but high levels of aluminum and silicon oxides, which in-

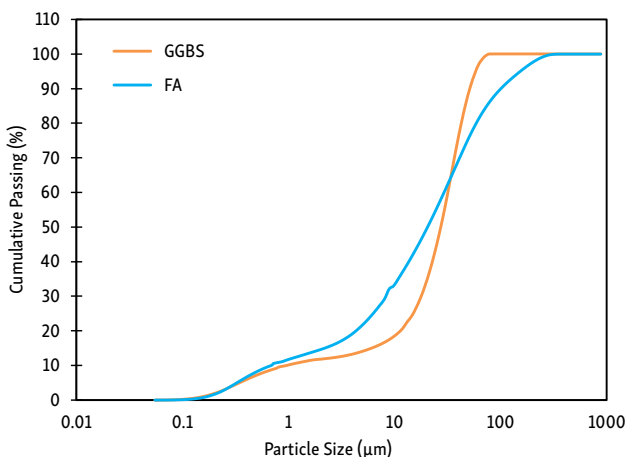


Figure 1. Particle size distribution of FA and GGBS

teract with an alkaline solution to form geopolymer paste (Lloyd & Rangan, 2010). The FA used in this study met the requirements of ASTM C618-19 (ASTM International, 2019).

GGBS, a by-product of steel and iron production, is generated by the fusion of limestone, iron ore, and coke to produce molten iron and slag. GGBS, is also referred as 'slag cement' (Suresh & Nagaraju, 2015), comprises a significant proportion of amorphous calcium, silica, and alumina. The rapid solidification of molten slags through high-pressure water jets results in the production of GGBS (Ahmad et al., 2022).

2.1.2. Aggregates

Steel slag aggregate (SSA) and crushed granite aggregate (CGA) with a size range of 10–19 mm were employed in the fabrication of GPC specimens. SSA is considered an industrial by-product, while CGA is classified as natural aggregate. CA was substituted with PKS-BC, a processed aggregate. According to BS 812-112 (BSI, 1990), the aggregate impact values for SSA and CGA were 4.49 and 7.41, respectively. Both are classified as exceptionally strong. SSA demonstrated 65% higher toughness than CGA. Table 1 presents the relative density and absorption values of the three types of CA utilized in the GPC, following ASTM C127 (ASTM International, 2024).

From Table 1, PKS-BC demonstrated the highest absorption value, followed by SSA and CGA. The notable absorption capability of the material can be attributed to its molecular structure, morphology, and large surface area (Piccolo et al., 2021).

Table 1. Relative density (Specific Gravity) and absorption of CA

| Coarse Aggregate (CA) | Relative density (Saturated-Surface-Dry) | Relative density (Oven-Dry) | Absorption (%) |
|-----------------------|--|-----------------------------|----------------|
| SSA | 3.10 | 3.03 | 1.54 |
| CGA | 2.60 | 2.44 | 0.53 |
| PKS-BC | 1.49 | 1.30 | 12.03 |

Table 2. The bulk density (ASTM C29) and the effective porosity of CA

| Types of CA | Bulk density (kg/m ³) | Void content (%) | Specific yield (S_y), (%) | Specific retention (S_r), (%) | Effective porosity ($S_y + S_r$) |
|-------------|-----------------------------------|------------------|-------------------------------|-----------------------------------|------------------------------------|
| SSA | 2037.20 | 32.63 | 39.86 | 6.13 | 45.99 |
| CGA | 1626.70 | 33.20 | 38.00 | 2.82 | 40.82 |
| PKS-BC | 528.10 | 59.30 | 44.54 | 10.66 | 55.20 |

The bulk density is a crucial indicator of the distribution of aggregates and voids within the aggregates. From Table 2, SSA demonstrates the highest bulk density, followed by CGA, and then PKS-BC. The void content of PKS-BC is 81.73% and 78.61% higher than SSA and CGA respectively. Although the void content of CGA is higher than SSA by 1.75%, the effective porosity of SSA is 12.67% higher compared to CGA. PKS-BC, which exhibited the highest void content, showed 20.03% and 35.23% higher effective porosity than SSA and CGA, respectively. In terms of water retention ability denoted as S_r , PKS-BC retains 73.90% and 278.01% more water compared to SSA and CGA, respectively. All three types of CA demonstrated a superior ability to release water from their saturated state through gravitational drainage denoted as S_y : 550.24%, 1247.52%, and 317.83% for SSA, CGA, and PKS-BC, respectively, when compared with their respective S_r values. The relationship between S_y and S_r indicates that not all porous spaces in porous materials are effective in holding liquid or allowing liquid to flow (Montes et al., 2005).

2.1.3. Alkaline activators

This research utilized three types of alkaline activators. The first type involved a mixture of commercial SS and 10M NaOH. The specific gravity values for commercial SS and NaOH were 1.67 and 1.33, respectively. The chemical composition of commercial SS included Na₂O (14.7%), SiO₂ (29.4%), and water (55.9%), with a silica modulus (M_s) of 2. Matinfar and Nychka (2023) noted that commercial SS typically exhibit M_s values ranging from 1.6 to 3.75, with silica concentrations typically falling between 25–35 wt%. The second activator type examined in this study was a combination of RHA-based IHS with 10M NaOH. Lastly, the research explored the use of a Hybrid SS activator consisting of 50% commercial SS and 50% TPOFA-based IHS with 10M NaOH. The content of Na₂O in 10M NaOH is approximately 15% by mass and the purchased NaOH powder was diluted cautiously in the lab. The chemical composition of raw RHA/TPOFA was determined through XRF analysis, and the findings are detailed in Table 3.

For the preparation of finer-sized POFA, the following methods were conducted as demonstrated in Figure 2. POFA was oven-dried at 105 °C for 24 hours, sieved using a 300-micron IS sieve, and were placed in the Los Angeles machine to guarantee 60,000 cycles. RHA was procured in the powdered form and then ground to finer size in the Los Angeles machine for 60,000 cycles too.

The POFA underwent additional treatment in a furnace at 500 °C for 2 hours to eliminate any residual carbon, resulting in the formation of treated POFA (TPOFA).

Table 3. The chemical composition of RHA and TPOFA

| Chemical composition | RHA | TPOFA |
|--------------------------------|-------|-------|
| SiO ₂ | 90.10 | 59.80 |
| Al ₂ O ₃ | 0.48 | 1.28 |
| CaO | 1.75 | 9.16 |
| Fe ₂ O ₃ | 0.95 | 5.28 |
| K ₂ O | 3.33 | 14.20 |
| SO ₃ | 0.37 | 1.20 |
| MgO | 0.31 | 2.66 |
| P ₂ O ₅ | 2.14 | 5.20 |

**Figure 2.** Procedure of preparing finer POFA

Subsequently, the isolation of IHS was carried out at 80 °C using a hydrothermal method with the help of a hot plate and stirrer. Hydrothermal method is known for its efficacy in extracting SS from industrial by-products (Alnahhal et al., 2023). At high temperatures, it promotes Brownian motion and depolymerization of silicate species although the gelation of base-catalyzed gel is less prominent than acid-catalyzed gels (Matinfar & Nychka, 2023). TPOFA, possessing a greater overall surface area, was selected over POFA to enhance the interaction between FA particles and the alkali activators (Hadi et al., 2018). The stirring was set for 2 and 4 hours for RHA and TPOFA-based mixture to yield respective IHS. After which, the attained IHS of both types, were let to cool down before it was mixed with 10M NaOH for casting of GPC.

The Hybrid SS synthesis was necessitated by the limitations in achieving adequate strength when POFA was used directly as SS in GPC. Consequently, TPOFA, known for its higher surface area than POFA was employed for the IHS extraction using hydrothermal method as depicted in Figure 3. A Hybrid SS approach was devised utilizing TPOFA, where a blend of 50% commercial SS and 50% TPOFA-based IHS underwent a reaction with 10M NaOH during casting. This method plays a crucial role in reducing the dependency on commercial SS.

The IHS extracted from RHA and TPOFA was subjected to chemical composition analysis using XRF, density testing using an electronic balance, and viscosity testing using an NDJ Digital Brookfield Rotational Viscometer. Rotor size 4 (#4) was employed in the viscometer, operating at 30 rpm for the viscosity test. The chemical composition of raw materials and IHS extracted from RHA and TPOFA was analyzed using XRF spectroscopy. For XRF test, the extracted IHS from RHA and TPOFA was oven-dried at 60 °C for 24 hours. Subsequently, the dried specimens were cooled, ground, and sieved to a particle size below 63 microns. To enhance the precision of the XRF test, pelletization of sample was done by compressing 8g of dried, powdered IHS under force to form pellets as depicted in Figure 4. XRF analysis was performed under vacuum conditions to mitigate the influence of helium gas on the pelletized specimen and improve the accuracy of the results (Bran-Anleu et al., 2018).

From Table 4, the density of commercial SS was 11.33%, 7.46%, and 3.60% higher than the density of RHA-based IHS, TPOFA-based IHS and Hybrid SS, respectively. The viscosity of commercial SS was found to be 5975.84%, 1811.26%, and 1364.36% higher than RHA-based IHS, TPOFA-based IHS, and Hybrid SS respectively. The viscosity of Hybrid SS is 314.91% and 30.52% higher than TPOFA-based IHS and RHA-based IHS, respectively. Additionally, TPOFA-based IHS exhibits a viscosity that is 217.90% higher than RHA-based IHS. The result is attributed to the mixing proportions and stirring conditions applied during the hydrothermal extraction of RHA and TPOFA as the viscosity increases monotonously with the concentration of the solution (Yang et al., 2008).



Figure 3. Extraction of IHS using hydrothermal method

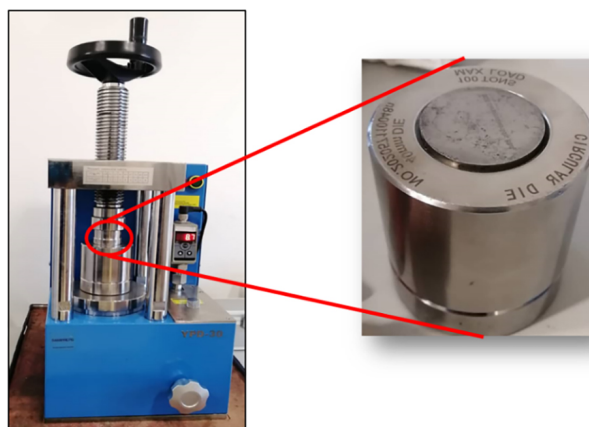


Figure 4. Pelletization of samples

It is imperative to identify the dissolved silica from these materials as geopolymerisation rely on the amount of dissolved oxides (Alnahhal et al., 2023). From Table 5, 22.30% of the 90.1% SiO_2 in RHA and 13.46% of the 59.80% SiO_2 in TPOFA dissolved when mixed with NaOH and water. The result demonstrates that NaOH: RHA: H_2O (1:1.4:2.7) ratio yields 35.27% more SiO_2 than NaOH: TPOFA: H_2O (1:4.5:1.5) ratio. The RHA and TPOFA-based IHS exhibits M_s of 5.51 and 2.99, respectively. The M_s of RHA-based IHS is 84.28% higher than TPOFA-based IHS. M_s is vital as at constant Na_2O , the compressive strength of geopolymer increases with an increasing amount of SiO_2 (Yadollahi et al., 2015). The chloride present was recorded negligible. Since chlorine-related-corrosion repair costs more compared to the combined cost of treating heart disease and cancer (Bran-Anleu et al., 2018), the absence of chloride in extracted IHS from RHA and TPOFA depicted positive results.

From Table 5, apart from SiO_2 and Na_2O , other oxides were identified during the extraction of IHS, as reported by Alnahhal et al. (2023). The proportions of Na_2O , SiO_2 and others in commercial SS, RHA-based IHS, TPOFA-based IHS, and Hybrid SS are depicted in Figure 5.

Table 4. Preparatory details of IHS and the viscosity of SS


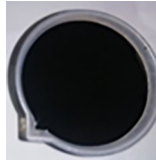
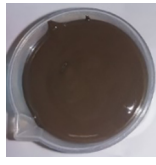

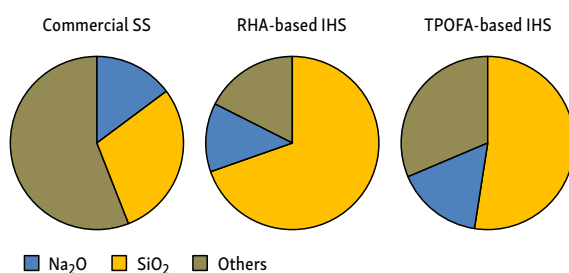
| Types of SS | Colour | Mix contents | Hours of stirring | Density (kg/m ³) | Average Torque (%) | Viscosity (mPa.s) |
|-----------------|--|--|-------------------|------------------------------|--------------------|-------------------|
| Commercial SS | Clear  | N/A | N/A | 1670 | 94.20 | 18329.00 |
| RHA-based IHS | Black  | NaOH: RHA: H ₂ O (1:1.4:2.7) | 2 | 1500 | 1.57 | 301.67 |
| TPOFA-based IHS | Brownish  | NaOH: TPOFA: H ₂ O (1:4.5:1.5) | 4 | 1554 | 4.90 | 959.00 |
| Hybrid SS | Brownish  | Commercial SS: TPOFA-based IHS (50:50) | N/A | 1612 | 6.13 | 1251.67 |

Table 5. XRF results of extracted IHS from RHA and TPOFA

| Chemical composition | RHA-based IHS | TPOFA-based IHS |
|--------------------------------|---------------|-----------------|
| SiO ₂ | 70.00 | 51.75 |
| Al ₂ O ₃ | 0.80 | 3.65 |
| CaO | 2.00 | 5.92 |
| Fe ₂ O ₃ | 1.00 | 3.24 |
| K ₂ O | 1.50 | 9.04 |
| SO ₃ | 0.20 | 0.83 |
| MgO | 0.15 | 3.73 |
| P ₂ O ₅ | 1.20 | 3.42 |
| Na ₂ O | 12.70 | 17.32 |
| Cl | 0.30 | 0.50 |

**Figure 5.** The proportion of Na₂O, SiO₂ and others in commercial SS, RHA-based IHS, and TPOFA-based IHS

2.2. Batching, casting, and curing procedure of GPC

Three types of SS (commercial SS, RHA-based IHS, Hybrid SS) with varying proportions of PKS-BC into GPC specimens were incorporated, along with two types of CA (SSA and CGA). The ratios of FA: GGBS and aggregate: binder were maintained at 0.7:0.3 and 7:1, respectively as depicted in Tables 6 and 7. The ratio of SS:10M NaOH was at 2.5 for all mixes. The mix design was established through weight batching to enhance accuracy and consistency (Olusola et al., 2012).

During the mixing process, the binders and their corresponding CA were initially mixed in a rotary-drum mixer. Subsequently, alkali activators were added and mixed for five minutes to ensure homogeneity. The aggregates employed were in SSD state to avoid water absorption from the concrete mixture during the casting phase (Lloyd & Rangan, 2010). The casting procedure is depicted in Figure 6.

2.3. Testing methods

2.3.1. Compressive strength test

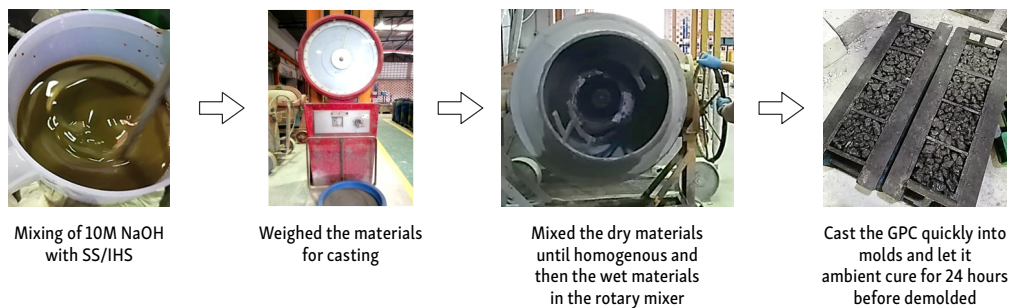
An average of three 100-mm cubes were tested for compressive strength test on days 1-, 7-, and 28-day complying with BS EN 12390-3 (BSI, 2019).

Table 6. Notations used to represent the GPC specimens

| Types of SS | Percentage of CA replaced with PKS-BC (%) | Types of CA | Designation |
|---|---|---------------------------------|----------------|
| Commercial SS | 0 | Steel Slag Aggregate (SSA) | C-SSA (C) |
| | 1 | | 1% BC-SSA (C) |
| | 3 | | 3% BC-SSA (C) |
| | 5 | | 5% BC-SSA (C) |
| | 10 | | 10% BC-SSA (C) |
| Commercial SS | 0 | Crushed Granite Aggregate (CGA) | C-CGA (C) |
| | 1 | | 1% BC-CGA (C) |
| | 3 | | 3% BC-CGA (C) |
| | 5 | | 5% BC-CGA (C) |
| RHA-based IHS | 0 | Steel Slag Aggregate (SSA) | C-SSA (R) |
| | 1 | | 1% BC-SSA (R) |
| | 5 | | 5% BC-SSA (R) |
| RHA-based IHS | 0 | Crushed Granite Aggregate (CGA) | C-CGA (R) |
| | 1 | | 1% BC-CGA (R) |
| | 5 | | 5% BC-CGA (R) |
| Hybrid SS (50% commercial SS + 50% TPOFA-based IHS) | 0 | Steel Slag Aggregate (SSA) | C-SSA (H) |
| | 1 | | 1% BC-SSA (H) |
| | 5 | | 5% BC-SSA (H) |
| Hybrid SS (50% commercial SS + 50% TPOFA-based IHS) | 0 | Crushed Granite Aggregate (CGA) | C-CGA (H) |
| | 1 | | 1% BC-CGA (H) |
| | 5 | | 5% BC-CGA (H) |

Table 7. Mix design to fabricate the GPC specimens in terms of kg/m³

| Types of specimens | Material content (kg/m ³) | | | | | |
|---------------------|---------------------------------------|--------|--------|-------|---------------|--------|
| | CA | FA | GGBS | NaOH | Commercial SS | IHS |
| SSA (Commercial SS) | 2369.01 | 236.90 | 101.53 | 48.35 | 120.87 | N/A |
| CGA (Commercial SS) | 2065.47 | 206.55 | 88.52 | 42.15 | 105.38 | N/A |
| SSA (RHA-based IHS) | 2369.01 | 236.90 | 101.53 | 48.35 | N/A | 120.87 |
| CGA (RHA-based IHS) | 2369.01 | 236.90 | 101.53 | 48.35 | N/A | 120.87 |
| SSA (Hybrid SS) | 2354.86 | 235.49 | 100.92 | 48.06 | 60.07 | 60.07 |
| CGA (Hybrid SS) | 2054.70 | 205.47 | 88.06 | 41.93 | 52.42 | 52.42 |

**Figure 6.** Casting procedure of GPC

2.3.2. Porosity test

Porosity test was assessed using the average values of two cylindrical specimens measuring 100 × 200 mm on day 28, complying with ASTM C1754 (ASTM International, 2021).

2.3.3. Infiltration rate test

The infiltration rate test was performed in situ on the hardened GPC by following the guidelines outlined in ASTM

C1701 (ASTM International, 2023) on day 28. A permeable paver, measuring 400 × 400 × 50 mm, was studied for infiltration property of the GPC specimen by placing a 300 mm circular ring at the center of the specimen. A standard 300-mm-diameter single-ring was chosen as it has similar results to a more involved double-ring embedded infiltration test. The ring was secured on the GPC surface to prevent lateral leakage during the infiltration test as depicted in Figure 7.



Figure 7. Infiltration test on GPC paver

2.3.4. Microstructural test

For the microstructural analysis, the samples were ground and sieved for FESEM-EDX, XRD and XRF analysis.

2.3.5. Ultra-violet (UV)-2600 spectrophotometer test

Urban Heat Island (UHI) impacts the environment negatively; however, measuring the albedo of pavement is difficult as it depends on the size of the specimen, variation in the solar input, and background interference (Sen et al., 2019). Thus, a spectroscopy test was conducted using a UV-2600 spectrophotometer as depicted in Figure 8, to understand the light reflectance of the powdered specimens.



Figure 8. UV-2600 spectrophotometer

3. Results and discussion

3.1. Compressive strength result

The compressive strength test results of all tested specimens are shown in Figure 9. These results are within the requirement of 2.8 to 28 MPa as recommended by the ACI Committee 522 (2023). The presence of pozzolanic materials like FA which consist of active SiO_2 and Al_2O_3 encourages the formation of calcium aluminate silicate hydrate (C–A–S–H) and sodium aluminate silicate hydrate (N–A–S–H) which densifies the matrix and results in higher strength and better durability (Fanghui et al., 2015).

3.1.1. Effect of the different types of CA on the compressive strength of GPC

From Figure 9, the compressive strength of SSA-based GPC specimens is relatively higher than the CGA-based GPC samples for all types of GPC specimens. This finding is attributed to the higher toughness and shape of SSA compared to CGA, proven through the AIT result.

3.1.2. Effect of RHA-based IHS on the compressive strength of GPC

Based on the test results as shown in Figure 9, the 28-day compressive strength of GPC prepared using RHA-based IHS increased by 17.20% and 2.75% for 1% BC, and 5% BC compared to the commercial SS-based GPC; in contrast, the CGA-based GPC had a significant increase in the strength with an increment of 73.05%, 62.34%, and 43.27%, respectively for C, 1% BC and 5% BC compared to the commercial SS-based GPC. The positive result could be attributed to the 138.10% higher SiO_2 in RHA-based IHS than commercial SS. The high amount of silica in the RHA tends to improve the compressive strength and reduce the expansions caused by alkali-silica reaction (ASR) although it was highlighted that this mitigation is influenced by the rice husk particle size (Khan et al., 2020). The

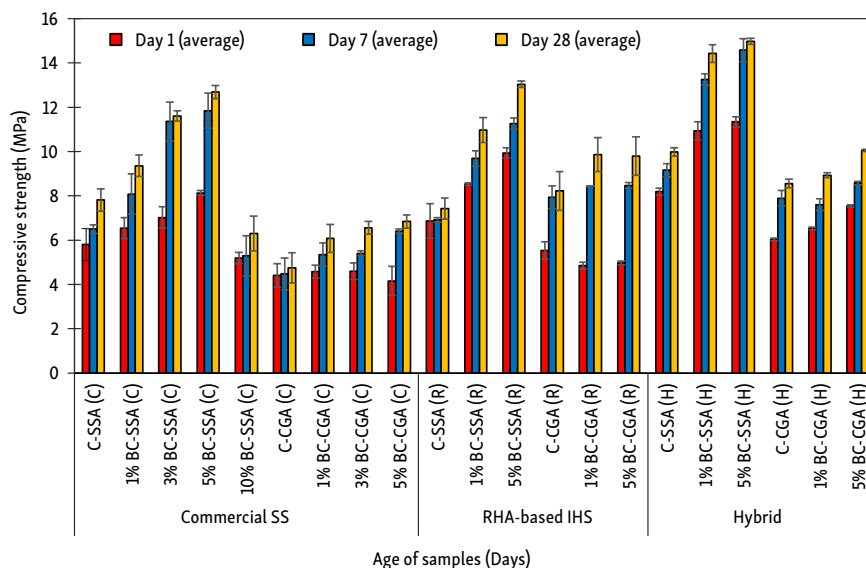


Figure 9. Compressive strength test results on 1-, 7-, and 28-day

RHA-based IHS specimens showed better strength than commercial SS-based specimens.

3.1.3. Effect of Hybrid SS on the compressive strength of GPC

It can be seen from Figure 9, that the 28-day compressive strength for Hybrid SS-based GPC specimens using SSA were found higher by 27.91%, 54.17%, and 18.05% compared to commercial SS-based GPC of C, 1% BC, and 5% BC, respectively. Furthermore, the Hybrid SS-based GPC specimens with CGA increased by 80.21%, 46.88% and 46.93% in comparison to commercial SS-based GPC of C, 1% BC and 5% BC, respectively. The average strength development in Hybrid SS-based GPC specimen was found to be relatively higher than commercial SS and RHA-based GPC.

In Hybrid SS-based GPC specimens, the strength is assumed to be developed from commercial SS and TPOFA-based IHS. NaOH ions can dissociate commercial SS quickly and form quick bonding between SiO_2 and Al_2O_3 species according to Alnahhal et al. (2023). The ease of Si dissolution takes place in an environment with higher pH (Nguyen, 2021) but depends on the Si content of the material too. TPOFA-based IHS possess high M_s and Si content which elevates the strength in GPC specimens. The high strength in GPC from Hybrid SS is attributed to the contribution of two sources of SS: commercial SS and TPOFA-based IHS.

3.1.4. Effect of PKS-BC on the compressive strength of GPC

The increment of compressive strength across the GPC specimens as the PKS-BC content increased, suggested that PKS-BC contributed to the strength development apart from the pozzolans. The trend is depicted in Figure 9.

The strength improved until when CA was substituted by 5%wt of PKS-BC in GPC, beyond which the organic matter (OM) appeared deleterious as demonstrated by 10% BC-SSA (C). The observed increase in compressive strength in the research can be ascribed to the filler effect of PKS-BC in the GPC, as indicated by Piccolo et al. (2021). A notable reduction in strength was noted when more than 5% BC was incorporated into the commercial SS-based GPC with SSA. This decrease could be linked to the aggregation effect or the potential creation of local voids along and around the interfacial zone of the concrete, as discussed by Qin et al. (2021). The structure and brittleness of carbonaceous particles, as emphasized by Tan et al. (2022), play a role in this phenomenon. The study's results indicate a critical threshold at which PKS-BC can enhance the GPC's increment; however, surpassing this limit may have an adverse impact on concrete.

Overall, the commercial SS and RHA-based specimens depicted quick strength development while Hybrid SS-based specimens depicted a stable strength development over the days when CA was replaced with PKS-BC up to 5% by weight, as depicted in Figure 9. RHA-based IHS showed a positive increment then commercial SS-based GPC specimens due to its rich silica content. Hybrid SS-based GPC specimens had positive and negative increments than commercial SS-based GPC specimens due to the weak pozzolanic property of TPOFA-based IHS incorporated in the Hybrid SS, amidst possessing better M_s than commercial SS.

3.2. Porosity test result

From Figure 10, it can be observed that the porosity as per ASTM C1754 (ASTM International, 2021), falls within the range of 33–47%. As the content of PKS-BC increases across the samples made of the same SS and CA, the po-

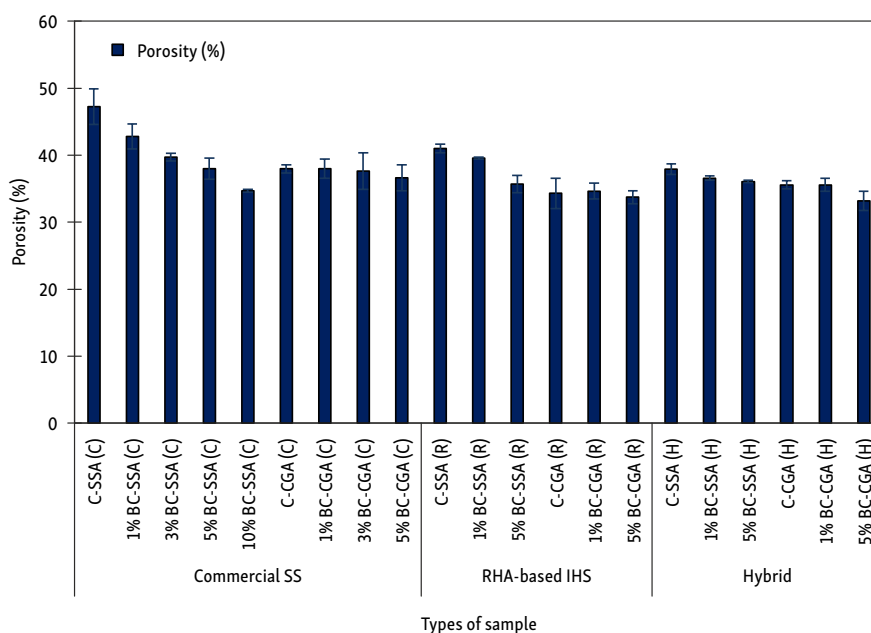


Figure 10. Porosity (%) of GPC specimens

rosity tend to decrease minimally overall. This is because, although BC is known for its ability to absorb water up to six times its weight, it exhibits lower open porosity and fills up pores as fillers when incorporated into geopolymers (Piccolo et al., 2021). On the other hand, Gupta et al. (2020) stated that water absorption by BC occurs only during the casting stage. This clarifies why BC being a porous matter, having a higher absorption value compared to SSA and CGA, does not seem to increase the porosity value in the samples.

3.3. Infiltration rate test results

The determination of infiltration rates in PC and pervious pavement systems is crucial for predicting the drainage performance of the system (Lederle et al., 2020). The infiltration capacity of GPC is influenced by factors such as aggregate size and mixture density (Obla, 2010), while the relationship between flowability and porosity is dependent on the distribution of pore sizes (Yazdani & Singh, 2013). In PC, the infiltration rate typically falls within the range of 0.001 to 0.012 m/s (Lederle et al., 2020; da Costa et al., 2021). However, deviations from this range, as illustrated in Figure 11, can be attributed to the use of larger-sized CA in GPC specimens, which create larger infiltration pathways. Ahmed and Hoque (2020) have shown that employing larger-sized aggregates leads to increased voids, higher porosity, and improved water flow within the concrete matrix. A clean, unobstructed surface facilitates high infiltration rates, with vertical water movement observed without any lateral seepage through the GPC.

Figure 11 illustrates the minimal difference in infiltration rate outcomes among different GPC specimens. The

results suggest that infiltration rates remained relatively consistent across various types of GPC specimens, predominantly ranging from 0.022 to 0.028 m/s. This indicates that the replacement of CA with PKS-BC did not significantly impede water infiltration. As highlighted by Tan et al. (2022), when small voids become saturated with water, larger inter-aggregate gaps act as the primary pathways for water absorption. This suggests that the inclusion of BC does not notably impact the secondary water absorption rate of PC or modify the infiltration characteristics of concrete. Therefore, it is apparent that the incorporation of PKS-BC did not exhibit any noticeable influence on the porosity or infiltration properties.

The absence of fine aggregates in the concrete led to empty spaces within the solidified structure, which enabled water to percolate rapidly through the concrete mixture (Luck et al., 2006) as shown in Figure 12. The larger voids, influenced by the CA size in this research, encouraged quicker infiltration.



Figure 12. Infiltration test of GPC

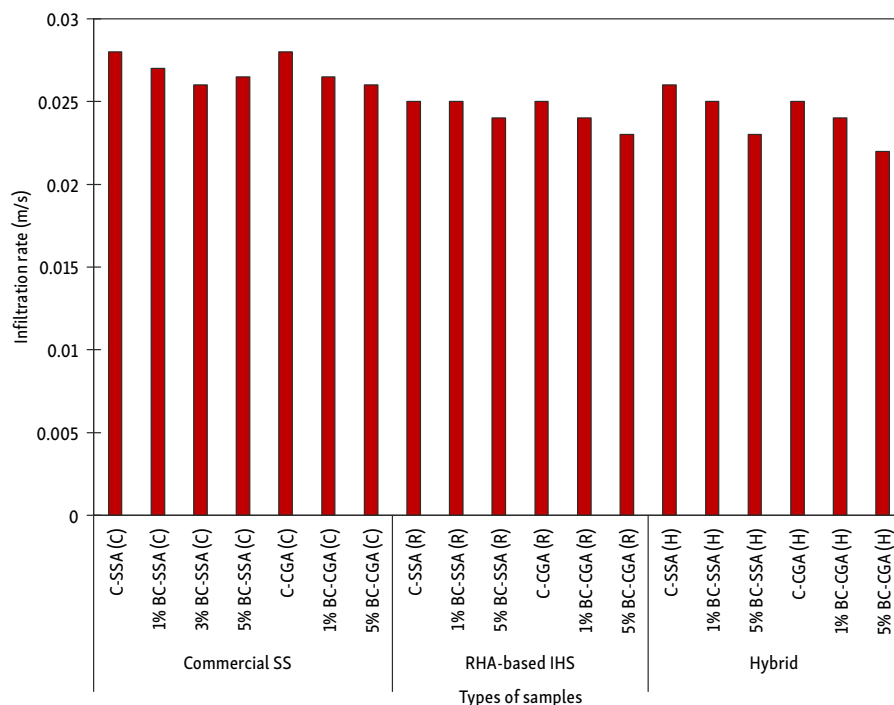


Figure 11. The infiltration test result as per ASTM C1701 (ASTM International, 2023)

3.4. Microstructural tests

3.4.1. FESEM-EDX test

The morphology exhibits the presence of PKS-BC, identifiable by its structure characterized by abundant fibrous macropores. Suman et al. (2017) observed distinct surface morphologies resulting from different feedstocks, with various types of BC showing differences. The black and white surfaces correspond to solid surfaces and void spaces, respectively. Pyrolyzed and unpyrolyzed BC display noticeable differences in macropores, as illustrated in Figure 13.

Figure 14 illustrates that both C-SSA (C) and 5% BC-SSA (C) comprised some untreated FA particles. Unreacted FA particles lead to an increased void content and results in weaker compressive strength (Alnahhal et al., 2022).

Figure 15 indicates the spongy structures of PKS-BC under different magnifications. PKS-BC depicts macropores, providing free spaces for air (Satriawan et al., 2021). Concrete particles can be seen filling up the pore spaces. This is because pyrolyzed BC provides a higher surface area for bonding to take place (Leng et al., 2021), yielding a better compressive strength in GPC as can be observed in Figure 9. The higher the PKS-BC content in all types of GPC samples (up to 5%wt substitution of CA with PKS-BC), the higher is the compressive strength test result.

From Table 8, carbon comprised the highest proportion of PKS-BC with a whopping 90.47% when selected spots from EDX images were analyzed, as shown in Figure 16. The content of Si is relatively low in PKS-BC at 0.6%, as according to Nguyen (2021), Si is subjected to dehydration, volatilization, condensation, slagging, and crystalliza-

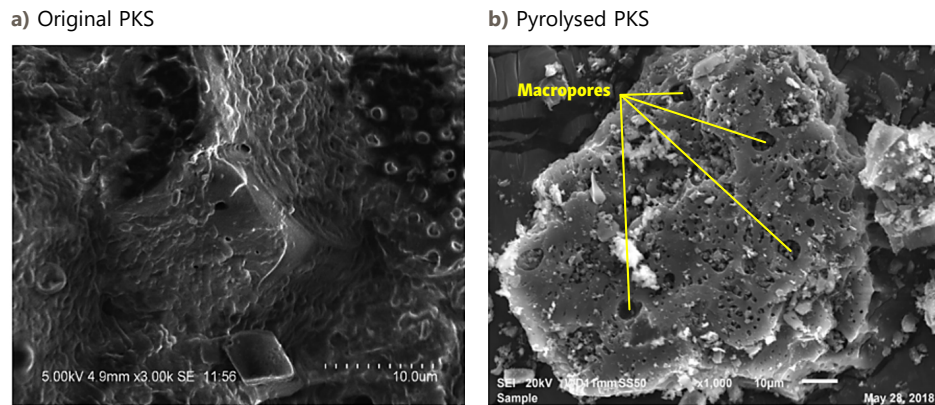


Figure 13. Microstructural observation of original and pyrolyzed PKS-BC (Kong et al., 2019)

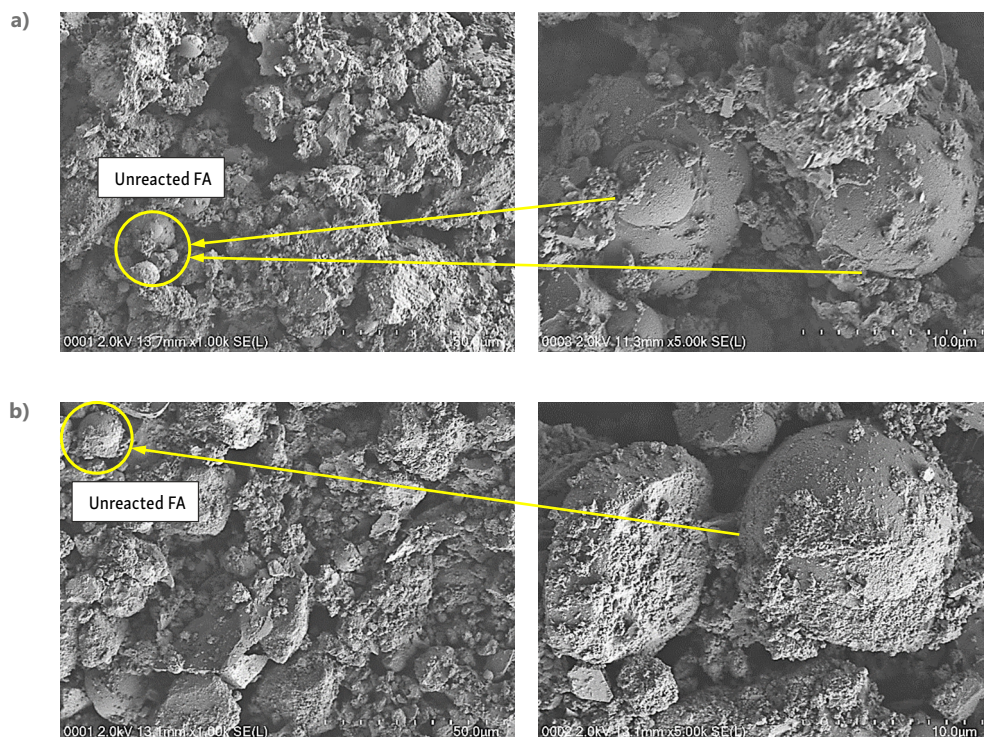


Figure 14. FESEM result: a – C-SSA (C); b – 5% BC-SSA (C) specimen

tion under pyrolysis. All elemental composition increased in 5% BC-SSA (C) when compared with PKS-BC, except for C content. The doubled content of elements like Na, Al, Si, Ca, and K in 5% BC-SSA (C) from PKS-BC could be attributed to the formation of C-A-S-H and N-A-S gels during geopolymerization of GPC specimens. FA and GGBS tend

to accelerate the formation of geopolymerisation to form N-A-S-H and C-A-S-H gels which form bonding between unreacted binder particles with polymer particles, filling the voids and yielding in dense microstructure (Liu et al., 2024). Thus, FA and GGBS in the presence of PKS-BC yields in higher compressive strength as depicted in Figure 9.

Table 8. Average elemental composition of PKS-BC, C-SSA (C), and 5% BC-SSA (C) under FESEM-EDX analysis

| Elements | | C | O | Si | Ca | Al | K | Fe | Na |
|----------------------------|---------------|-------|-------|------|------|------|------|------|------|
| Average atomic content (%) | PKS-BC | 90.47 | 8.22 | 0.60 | 0.35 | 0.14 | 0.09 | 0.04 | 0.04 |
| | 5% BC-SSA (C) | 58.66 | 28.47 | 5.18 | 1.12 | 4.72 | 0.25 | 0.40 | 1.17 |

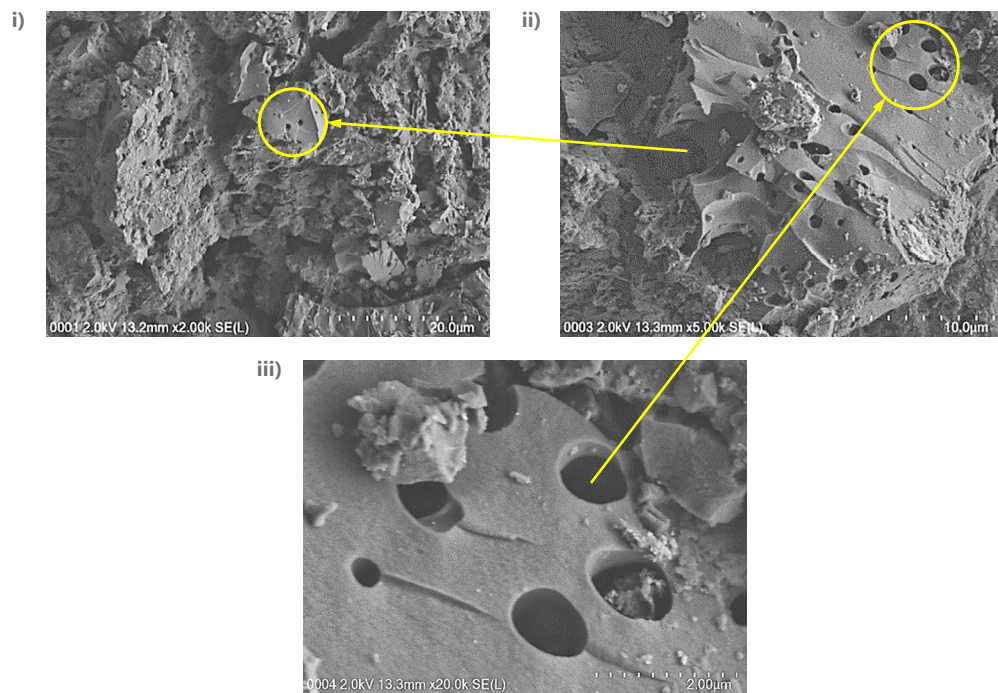


Figure 15. FESEM images of PKS-BC at i) 2k, ii) 5k, and iii) 20k magnifications

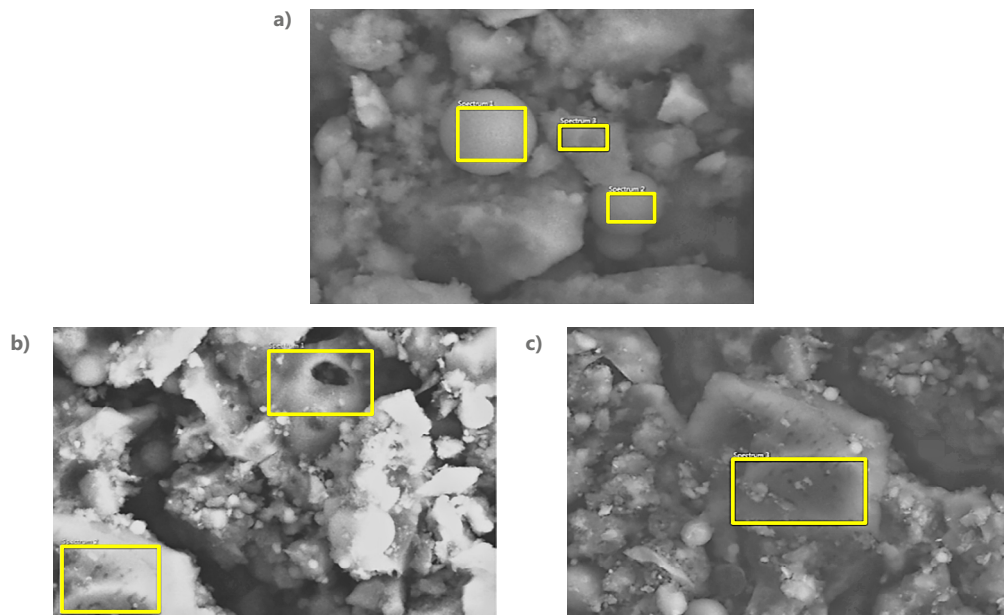


Figure 16. Chosen spots on EDX images for elemental composition: a – PKS-BC; b and c – 5% BC SSA (C)

3.4.2. X-Ray Diffraction (XRD) analysis

Figure 17 shows the XRD result of commercial SS, RHA-based, and Hybrid SS-based GPC specimens. The major crystalline peaks such as Quartz (SiO_2) accompanied with geopolymer gel of N-A-S of analcime minerals were observed at diffraction angles 2θ of 26.64° and 26.65° , respectively. The presence of quartz in XRD results reflects the mineralogical composition of the sample and provides insights into the geological characteristics of the material (Millogo et al., 2008). The existence of these compounds was analyzed by using High Score Plus software version 3 and the pattern match was 100%. The major crystalline peaks and their characteristics are illustrated in Table 9. The presence of calcium carbonate crystal, calcite (CC) was observed at 2θ of 29.39° in all the specimens. In this study, due to the pervious nature of GPC, it could be perceived that the absorption of CO_2 from the atmosphere and reaction with CaO in GGBS and FA formed the calcite (CC) crystal. Besides, the interaction of the carbonaceous minerals and PKS-BC yields in carbonate minerals like Calcite too (Kong et al., 2019). The intensity of CC crystal was higher in Hybrid SS-based GPC than in specimens with RHA-based IHS. Replacing CA with PKS-BC at 1% and 5% in specimens enhanced the 28-day compressive strength due to the corresponding improvement in GPC strength governed by the product of N-A-S gel in XRD plot of 1% BC and 5% BC for specimens with RHA-based IHS.

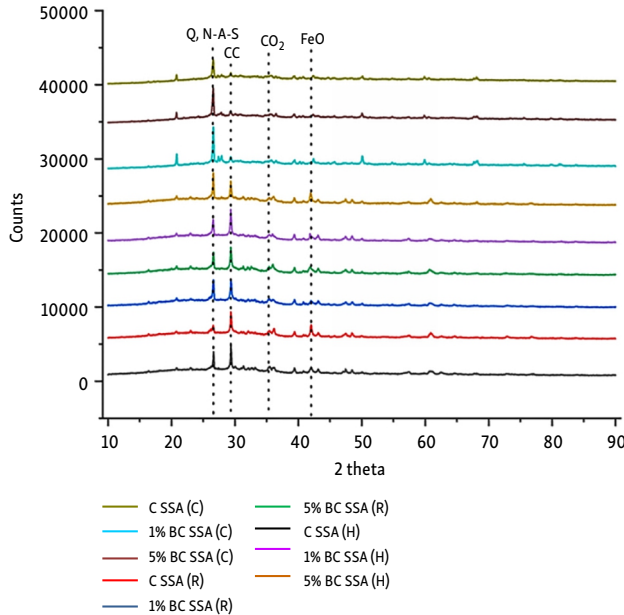


Figure 17. XRD analysis of GPC

Table 9. Major crystalline peaks and their characteristics

| S. No | Compounds | Chemical formula | Crystal structure | COD database |
|-------|-----------|------------------|-------------------|--------------|
| 1 | Quartz | SiO_2 | Hexagonal | 9013321 |
| 2 | Analcime | N-A-S | Orthorhombic | 9004013 |
| 3 | Calcite | CaCO_3 | Hexagonal | 9009667 |
| 4 | Wuestite | FeO | Cubic | 1011168 |

To deduce, control GPC specimens activated by commercial SS rather than IHS solution observed a lower intensity of CC, and CO_2 among all the mixes, which signified the absence of unreacted alkalis (NaOH and SS). By increasing the PKS-BC replacement level from 1% to 5%, the peak intensity of quartz (Q) and N-A-S gel gets reduced which indicates the enhanced polymerization reaction.

3.5. UV-2600 spectrophotometer result

The reflectance (%) analyzed using UV-2600 Spectrophotometer of selected specimens with varying content of PKS-BC and different types of SS are discussed in this section. The standard specimen kept in the cuvette prior to specimen testing was Barium Suphate (BaSO_4), served as the constant, which is crucial for data comparison. BaSO_4 is selected as the standard reference material due to its cost-effectiveness, high reflectivity, and consistent properties (Poh et al., 2019). A range of 200–800 nm wavelength was chosen for this test as 800 nm wavelength is optimal to measure the absorbance (Wang et al., 2017) and the human eyes can only perceive visible light ranging between 400–700 nm (Fan et al., 2022).

Figures 18 and 19 illustrate the light reflectance (%) of ground and sieved GPC specimens. The result is influenced by their respective refractive indices and color of the particles. The highlighted red bands in the graphs indicate the closeness towards the BaSO_4 the constant.

Since 63-micron-sized powder was used to test for light reflectivity, the overall reflectivity of GPC specimen was not detected in this study except for the fines present in the powder. The test results indicate that the powdered PKS-BC exhibited the lowest reflectivity (%) due to their dark color. Powdered GPC specimens, however demonstrated higher reflectivity than PKS-BC. The reflectance values of the GPC specimens ranged from 71% to 99.3% for RHA and Hybrid SS-based GPC across the 400–700 nm wavelengths, as illustrated in Table 10. The high reflectivity of the powdered species can be attributed to the light-colored binder used namely the GGBS.

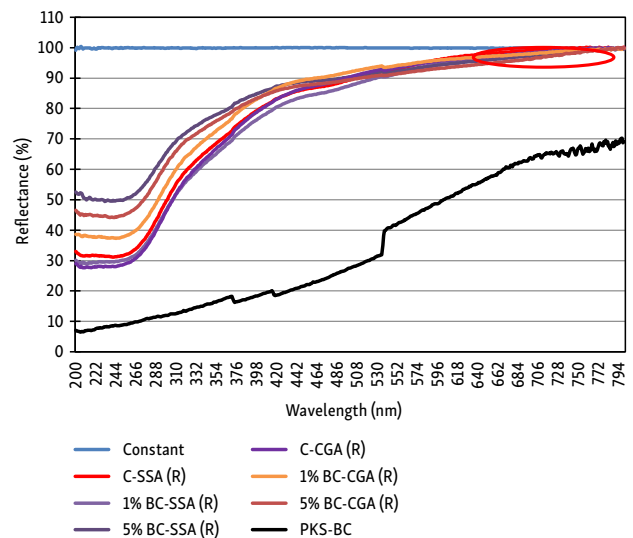
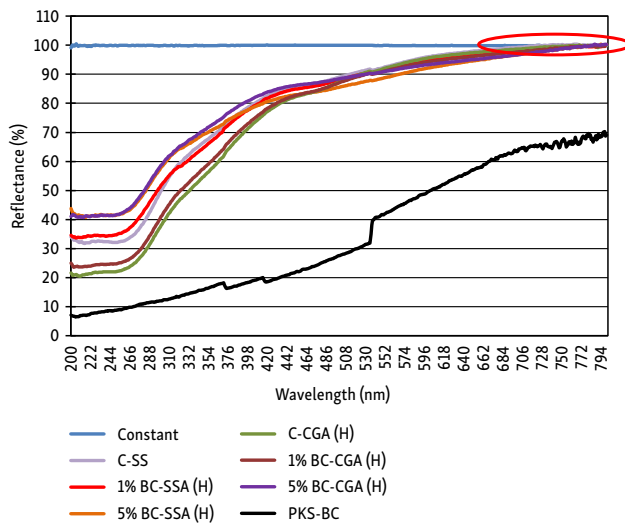


Figure 18. Reflectivity of powdered GPC with RHA-based HIS

Table 10. Reflectance (%) of specimens

| Reflectance of powder specimen from RHA based GPC | | | | | | |
|---|-----------|---------------|---------------|-----------|---------------|---------------|
| RHA based GPC | C-SSA (R) | 1% BC-SSA (R) | 5% BC-SSA (R) | C-CGA (R) | 1% BC-CGA (R) | 5% BC-CGA (R) |
| 400 nm | 79.61 | 76.68 | 85.05 | 79.20 | 83.37 | 83.57 |
| 700 nm | 99.07 | 98.24 | 97.30 | 98.23 | 98.03 | 96.33 |
| Reflectance of powder specimen from Hybrid SS based GPC | | | | | | |
| Hybrid SS | C-SSA (H) | 1% BC-SSA (H) | 5% BC-SSA (H) | C-CGA (H) | 1% BC-CGA (H) | 5% BC-CGA (H) |
| 400 nm | 79.00 | 77.61 | 78.04 | 71.85 | 73.42 | 81.02 |
| 700 nm | 99.21 | 98.19 | 96.71 | 98.60 | 97.60 | 96.64 |

**Figure 19.** Reflectivity of powdered GPC with Hybrid SS

Commonly, light-colored concrete is known to have superior solar reflectivity, contributing to a brighter environment (Sweeney et al., 2011). Additionally, brighter concrete enhances visibility, particularly at night, resulting in a potential 30% reduction in lighting requirements (Sweeney et al., 2011). Mallick et al. (2015) illustrated that a decrease in pavement temperature extended the pavement's lifespan by 3–4 times. This research underscores the rationale for incorporating bright-colored GGBS in the study. According to Sanjuán et al. (2021), concrete pavements generally demonstrate higher reflectivity levels than asphalt pavements.

4. Conclusions

In the making of sustainable GPC, three types of aggregates were employed, including conventional CGA, steel-based SSA, and pyrolyzed PKS-BC. PKS-BC was used as a replacement for SSA and CGA in this study. FA and GGBS, were used as binders in the GPC. Additionally, RHA and TPOFA were used as alternative silicate sources in the development of SS. A hydrothermal technique was applied in this study to extract IHS from RHA and TPOFA at 80 °C, facilitating the dissociation of Si-O-Si bonds by NaOH ions. The innovative aspect of this study is the development of a Hybrid SS that combines 50% commercial SS with 50% TPOFA-based IHS. The application aspect of this

study will be as pavement for pedestrian walkways as PC possess lower compressive strength when compared with conventional concrete.

Based on the research, the following conclusions have been drawn:

- The hydrothermal method is viable for extracting sodium silicate from RHA and TPOFA.
- The strength of GPC directly depended on the mix proportions of Na₂O, H₂O, and RHA/TPOFA, and the stirring duration to extract SS.
- RHA-based IHS yielded a better compressive strength compared to the TPOFA-based IHS due to the high content of silica, allowing more silica dissolution by the NaOH ions. Thus, the Hybrid SS using commercial SS and TPOFA was synthesized to improve the compressive strength in the GPC specimen.
- The compressive strength of the GPC specimens prepared using Hybrid SS was found to be at par with the specimens of commercial SS and RHA based HIS.
- The type of CA had influence on the compressive strength in the GPC. SSA-based specimens depicted higher compressive strength compared to CGA-based PC due to the higher toughness, shape, and bond between the paste and the SSA.
- The incorporation of PKS-BC up to a threshold level of 5% in GPC promotes a better compressive strength as it acts as a filler and possesses high stability in structure with its higher surface area due to its spongy structure.
- The light reflectivity of the powder of GPC specimens was greater than powder of PKS-BC; the high reflectivity of the ground GPC powder is attributed to the fine-sized binders that scatter the light rays in various directions. In addition, the white coloured GGBS has an influence on the reflectance.

For the future work:

- Mechanical test results beyond 28 days can be carried out as geopolymer concrete may exhibit varying behaviour over longer period.
- The ratio which requires lesser usage of NaOH in the preparation of IHS can be further experimented.
- The bond strength of GPC with commercial SS vs IHS can be further studied.
- The quantification of carbon and environmental footprint can be studied.
- The abrasion resistance of the GPC samples can be measured.

Acknowledgements

The authors express their gratitude to the Ministry of Higher Education, Malaysia for the financial support through the Fundamental Research Grant Scheme (FRGS) bearing project grant No. Ref: FRGS/1/2022/TK01/UM/02/4 awarded to the Principal Investigator, Professor Ir. Dr. Ubagaram Johnson Alengaram.

Conflict of interest

The authors declare that they have no known competing financial interests or personal relationships that could have appeared to influence the work reported in this paper.

References

- ACI Committee 522. (2023). *Pervious concrete*.
- Ahmad, J., Kontoleon, K. J., Majdi, A., Naqash, M. T., Deifalla, A. F., Ben Kahla, N., Isleem, H. F., & Qaidi, S. M. A. (2022). A comprehensive review on the ground granulated blast furnace slag (GGBS) in concrete production. *Sustainability*, 14(14), Article 8783. <https://doi.org/10.3390/su14148783>
- Ahmed, T., & Hoque, S. (2020). Study on pervious concrete pavement mix designs. *IOP Conference Series: Earth and Environmental Science*, 476(1), Article 012062. <https://doi.org/10.1088/1755-1315/476/1/012062>
- Alnahhal, A. M., Alengaram, U. J., Yusoff, S., Darvish, P., Srinivas, K., & Sumesh, M. (2022). Engineering performance of sustainable geopolymer foamed and non-foamed concretes. *Construction and Building Materials*, 316, Article 125601. <https://doi.org/10.1016/j.conbuildmat.2021.125601>
- Alnahhal, A. M., Johnson Alengaram, U., Shazril Idris Ibrahim, M., K. H. Radwan, M., & Ayough, P. (2023). Extraction of home brewed sodium silicate from palm oil fuel ash and its effect on alkali activated materials. *Construction and Building Materials*, 407, Article 133440. <https://doi.org/10.1016/j.conbuildmat.2023.133440>
- Arun, A., & Chekravarty, D. (2022). Strength improvement techniques on pervious concrete. *Materials Today: Proceedings*, 52(Part 3), 1979–1985. <https://doi.org/10.1016/j.matpr.2021.11.624>
- ASTM International. (1997). *Standard test method for bulk density ("unit weight") and voids in aggregate* (ASTM C29/C29M-97).
- ASTM International. (2019). *Standard specification for coal ash and raw or calcined natural pozzolan for use in concrete* (ASTM C618-19).
- ASTM International. (2021). *Standard test method for density and void content of hardened pervious concrete* (ASTM C1754/C1754M-12).
- ASTM International. (2023). *Standard test method for infiltration rate of in place pervious concrete* (ASTM C1701/C1701M-17a).
- ASTM International. (2024). *Standard test method for relative density (specific gravity) and absorption of coarse aggregate* (ASTM C127-24).
- Bran-Anleu, P., Caruso, F., Wangler, T., Pomjakushina, E., & Flatt, R. J. (2018). Standard and sample preparation for the micro XRF quantification of chlorides in hardened cement pastes. *Microchemical Journal*, 141, 382–387. <https://doi.org/10.1016/j.microc.2018.05.040>
- British Standards Institution. (1990). *Testing aggregates – Part 112: Methods for determination of aggregate impact value (AIV)* (BSI 812-112:1990).
- British Standards Institution. (2019). *Testing hardened concrete – Compressive strength of test specimens* (BS EN 12390-3:2019).
- Cai, J., Liu, Z., Xu, G., Tian, Q., Shen, W., Li, B., & Chen, T. (2022). Mix design methods for pervious concrete based on the meso-structure: Progress, existing problems and recommendation for future improvement. *Case Studies in Construction Materials*, 17, Article e01253. <https://doi.org/10.1016/j.cscm.2022.e01253>
- da Costa, F. B. P., Haselbach, L. M., & da Silva Filho, L. C. P. (2021). Pervious concrete for desired porosity: Influence of w/c ratio and a rheology-modifying admixture. *Construction and Building Materials*, 268, Article 121084. <https://doi.org/10.1016/j.conbuildmat.2020.121084>
- Duxson, P., Provis, J. L., Lukey, G. C., Mallicoate, S. W., Kriven, W. M., & Van Deventer, J. S. (2005). Understanding the relationship between geopolymer composition, microstructure and mechanical properties. *Colloids and Surfaces A: Physicochemical and Engineering Aspects*, 269(1–3), 47–58. <https://doi.org/10.1016/j.colsurfa.2005.06.060>
- Fan, B., Zhang, C. X., Chi, J., Liang, Y., Bao, X. L., Cong, Y. Y., Yu, B., Li, X., & Li, G. Y. (2022). The molecular mechanism of retina light injury focusing on damage from short wavelength light. *Oxidative Medicine and Cellular Longevity*, 2022, Article 8482149. <https://doi.org/10.1155/2022/8482149>
- Fanghui, H., Qiang, W., & Jingjing, F. (2015). The differences among the roles of ground fly ash in the paste, mortar and concrete. *Construction and Building Materials*, 93, 172–179. <https://doi.org/10.1016/j.conbuildmat.2015.05.117>
- Georgiades, M., Shah, I. H., Steubing, B., Cheeseman, C., & Myers, R. J. (2023). Prospective life cycle assessment of European cement production. *Resources, Conservation and Recycling*, 194, Article 106998. <https://doi.org/10.1016/j.resconrec.2023.106998>
- Gupta, S., Kua, H. W., & Pang, S. D. (2020). Effect of biochar on mechanical and permeability properties of concrete exposed to elevated temperature. *Construction and Building Materials*, 234, Article 117338. <https://doi.org/10.1016/j.conbuildmat.2019.117338>
- Gupta, S., Kashani, A., Mahmood, A. H., & Han, T. (2021). Carbon sequestration in cementitious composites using biochar and fly ash – Effect on mechanical and durability properties. *Construction and Building Materials*, 291, Article 123363. <https://doi.org/10.1016/j.conbuildmat.2021.123363>
- Hadi, M. N. S., Al-Azzawi, M., & Yu, T. (2018). Effects of fly ash characteristics and alkaline activator components on compressive strength of fly ash-based geopolymer mortar. *Construction and Building Materials*, 175, 41–54. <https://doi.org/10.1016/j.conbuildmat.2018.04.092>
- Jadhav, R., Vyas, K., Gollapudi, B., Prajwal, & Anil, T. (2022). Reviewing the implementation of 'Thirsty concrete' in the urban areas. *Materials Today: Proceedings*, 64, 1000–1005. <https://doi.org/10.1016/j.matpr.2022.05.085>
- Kaur, M., Singh, J., & Kaur, M. (2018). Microstructure and strength development of fly ash-based geopolymer mortar: Role of nano-metakaolin. *Construction and Building Materials*, 190, 672–679. <https://doi.org/10.1016/j.conbuildmat.2018.09.157>
- Khan, K., Ullah, M. F., Shahzada, K., Amin, M. N., Bibi, T., Wahab, N., & Aljaafari, A. (2020). Effective use of micro-silica extracted from rice husk ash for the production of high-performance and sustainable cement mortar. *Construction and Building Materials*, 258, Article 119589. <https://doi.org/10.1016/j.conbuildmat.2020.119589>
- Kong, R., Li, J., Orban, C., Sabuncu, M. R., Liu, H., Schaefer, A., Sun, N., Zuo, X. N., Holmes, A. J., Eickhoff, S. B., & Yeo, B. T. T. (2019). Spatial topography of individual-specific cortical net-

- works predicts human cognition, personality, and emotion. *Cerebral Cortex*, 29(6), 2533–2551. <https://doi.org/10.1093/cercor/bhy123>
- Lederle, R., Shepard, T., & De La Vega Meza, V. (2020). Comparison of methods for measuring infiltration rate of pervious concrete. *Construction and Building Materials*, 244, Article 118339. <https://doi.org/10.1016/j.conbuildmat.2020.118339>
- Leng, L., Xiong, Q., Yang, L., Li, H., Zhou, Y., Zhang, W., Jiang, S., Li, H., & Huang, H. (2021). An overview on engineering the surface area and porosity of biochar. *Science of the Total Environment*, 763, Article 144204. <https://doi.org/10.1016/j.scitotenv.2020.144204>
- Lingyu, T., Dongpo, H., Jianing, Z., & Hongguang, W. (2021). Durability of geopolymers and geopolymer concretes: A review. *Reviews on Advanced Materials Science*, 60(1), 1–14. <https://doi.org/10.1515/rams-2021-0002>
- Liu, W., Feng, Q., Chen, W., & Deo, R. C. (2020). Stormwater runoff and pollution retention performances of permeable pavements and the effects of structural factors. *Environmental Science and Pollution Research*, 27(24), 30831–30843. <https://doi.org/10.1007/s11356-020-09220-2>
- Liu, M., Dai, W., Jin, W., Li, M., Yang, X., Han, Y., & Huang, M. (2024). Mix proportion design and carbon emission assessment of high strength geopolymer concrete based on ternary solid waste. *Scientific Reports*, 14(1), Article 24989. <https://doi.org/10.1038/s41598-024-76774-3>
- Lloyd, N. A., & Rangan, B. V. (2010). *Geopolymer concrete: A review of development and opportunities*. In C. Tam, K. Ong, S. Teng, & M. Zhang (Eds.), *35th Conference on Our World in Concrete & Structures: "The Challenge of Low Carbon Age"* (pp. 307–314). CI-Premier Pte Ltd.
- Luck, J. D., Workman, S. R., Higgins, S. F., & Coyne, M. S. (2006). Hydrologic properties of pervious concrete. *Transactions of the ASABE*, 49(6), 1807–1813. <https://doi.org/10.13031/2013.22301>
- Mallick, R. B., Li, H., Harvey, J., Myers, R., Veeraragavan, A., & Reck, N. (2015). Pavement life-extending potential of geosynthetic-reinforced chip seal with high-reflectivity aggregates. *Transportation Research Record: Journal of the Transportation Research Board*, 2474, 19–29. <https://doi.org/10.3141/2474-03>
- Matinfar, M., & Nychka, J. A. (2023). A review of sodium silicate solutions: Structure, gelation, and syneresis. In *Advances in Colloid and Interface Science*, 322, Article 103036. <https://doi.org/10.1016/j.cis.2023.103036>
- Mesghi, B., Beskopylny, A. N., Stel'makh, S. A., Shcherban', E. M., Mailyan, L. R., Shilov, A. A., El'shaeva, D., Shilova, K., Karalar, M., Aksoylu, C., & Özkılıç, Y. O. (2023). Analytical review of geopolymer concrete: Retrospective and current issues. *Materials*, 16(10), Article 3792. <https://doi.org/10.3390/ma16103792>
- Millogo, Y., Traoré, K., Ouedraogo, R., Kaboré, K., Blanchart, P., & Thomassin, J. H. (2008). Geotechnical, mechanical, chemical and mineralogical characterization of a lateritic gravels of Sapouy (Burkina Faso) used in road construction. *Construction and Building Materials*, 22(2), 70–76. <https://doi.org/10.1016/j.conbuildmat.2006.07.014>
- Mohajerani, A., Bakaric, J., & Jeffrey-Bailey, T. (2017). The urban heat island effect, its causes, and mitigation, with reference to the thermal properties of asphalt concrete. *Journal of Environmental Management*, 197, 522–538. <https://doi.org/10.1016/j.jenvman.2017.03.095>
- Montes, F., Valavala, S., & Haselbach, L. M. (2005). A new test method for porosity measurements of portland cement pervious concrete. *Journal of ASTM International*, 2(1), 1–13. <https://doi.org/10.1520/JAI12931>
- Nguyen, M. N. (2021). Potential use of silica-rich biochar for the formulation of adaptively controlled release fertilizers: A mini review. *Journal of Cleaner Production*, 307, Article 127188. <https://doi.org/10.1016/j.jclepro.2021.127188>
- Nurrudin, M. F., Haruna, S., Mohammed, B. S., & Sha'abanet, I. G. (2018). Methods of curing geopolymer concrete: A review. *International Journal of Advanced and Applied Sciences*, 5(1), 31–36. <https://doi.org/10.21833/ijaas.2018.01.005>
- Obla, K. H. (2010). Pervious concrete-An overview. *The Indian Concrete Journal*, 9–18.
- Olusola, K. O., Babafemi, A. J., Umoh, A. A., & Olawuyi, B. J. (2012). Effect of batching methods on the fresh and hardened properties of concrete. *International Journal of Research and Review in Applied Sciences (IJRRAS)*, 13(3), 773–779.
- Patankar, S. V., Ghugal, Y. M., & Jamkar, S. S. (2015). Mix design of fly ash based geopolymer concrete. In V. Matsagar (Ed.), *Advances in structural engineering* (pp. 1619–1634). Springer, New Delhi. https://doi.org/10.1007/978-81-322-2187-6_123
- Poh, A. H., Jamaludin, M. F., Fadzallah, I. A., Nik Ibrahim, N. M. J., Yusof, F., Adikan, F. R. M., & Moghavvemi, M. (2019). Diffuse reflectance spectroscopic analysis of barium sulfate as a reflection standard within 173–2500 nm: From pure to sintered form. *Journal of Near Infrared Spectroscopy*, 27(6), 393–401. <https://doi.org/10.1177/0967033519868241>
- Piccolo, F., Andreola, F., Barbieri, L., & Lancellotti, I. (2021). Synthesis and characterization of biochar-based geopolymer materials. *Applied Sciences*, 11(22), Article 10945. <https://doi.org/10.3390/app112210945>
- Qin, Y., Pang, X., Tan, K., & Bao, T. (2021). Evaluation of pervious concrete performance with pulverized biochar as cement replacement. *Cement and Concrete Composites*, 119, Article 104022. <https://doi.org/10.1016/j.cemconcomp.2021.104022>
- Sachet, W. H., & Salman, W. D. (2021). Geopolymer concrete, mortar, and paste: A review. *IOP Conference Series: Materials Science and Engineering*, 1076(1), Article 012108. <https://doi.org/10.1088/1757-899x/1076/1/012108>
- Sanjuán, M. Á., Morales, Á., & Zaragoza, A. (2021). Effect of precast concrete pavement albedo on the climate change mitigation in Spain. *Sustainability*, 13(20), Article 11448. <https://doi.org/10.3390/su132011448>
- Satriawan, A., Muhdarina, & Awaluddin, A. (2021). The utilization silica from oil fly ash as a raw material for paper filler. *Journal of Physics: Conference Series*, 2049, Article 012062. <https://doi.org/10.1088/1742-6596/2049/1/012062>
- Sen, S., Roesler, J., & King, D. (2019). Albedo estimation of finite-sized concrete specimens. *Journal of Testing and Evaluation*, 47(2), 738–757. <https://doi.org/10.1520/JTE20170059>
- Siddika, A., Mamun, M. A. Al, Alyousef, R., & Mohammadhosseini, H. (2021). State-of-the-art-review on rice husk ash: A supplementary cementitious material in concrete. *Journal of King Saud University – Engineering Sciences*, 33(5), 294–307. <https://doi.org/10.1016/j.jksues.2020.10.006>
- Soundararajan, E. K., & Vaiyapuri, R. (2021). Geopolymer binder for pervious concrete. *Gradjevinar*, 73(3), 209–218. <https://doi.org/10.14256/JCE.2440.2018>
- Srikanth, N., & Dakshina Murthy, N. R. (2021). Studies on infiltration rate of pervious concrete. In S. Chandrasekaran, S. Kumar, & S. Madhuri (Eds.), *Lecture notes in civil engineering: Vol. 135. Recent advances in structural engineering* (pp. 21–28). Springer, Singapore. https://doi.org/10.1007/978-981-33-6389-2_3
- Suman, S., Panwar, D. S., & Gautam, S. (2017). Surface morphology properties of biochars obtained from different biomass waste. *Energy Sources, Part A: Recovery, Utilization and Environmental Effects*, 39(10), 1007–1012. <https://doi.org/10.1080/15567036.2017.1283553>

- Suresh, D., & Nagaraju, K. (2015). Ground granulated blast slag (GGBS) in concrete – A review. *IOSR Journal of Mechanical and Civil Engineering (IOSR-JMCE)*, 12(4), 76–82.
- Sweeney, A., West, R. P., & O'Connor, C. (2011). *Parameters affecting the albedo effect in concrete*.
- Tambichik, M. A., Samad, A. A. A., Mohamad, N., Ali, A. Z. M., Mydin, M. A. O., Bosro, M. Z. M., & Iman, M. A. (2018). Effect of combining Palm Oil Fuel Ash (POFA) and Rice Husk Ash (RHA) as pozzolan to the compressive strength of concrete. *International Journal of Integrated Engineering*, 10(8), 61–67. <https://doi.org/10.30880/ijie.2018.10.08.004>
- Tan, T. H., Mo, K. H., Ling, T. C., & Lai, S. H. (2020). Current development of geopolymer as alternative adsorbent for heavy metal removal. *Environmental Technology and Innovation*, 18, Article 100684. <https://doi.org/10.1016/j.eti.2020.100684>
- Tan, K., Qin, Y., & Wang, J. (2022). Evaluation of the properties and carbon sequestration potential of biochar-modified pervious concrete. *Construction and Building Materials*, 314, Article 125648. <https://doi.org/10.1016/j.conbuildmat.2021.125648>
- Thomas, B. S., Yang, J., Bahurudeen, A., Chinnu, S. N., Abdalla, J. A., Hawileh, R. A., & Hamada, H. M. (2022). Geopolymer concrete incorporating recycled aggregates: A comprehensive review. *Cleaner Materials*, 3, Article 100056. <https://doi.org/10.1016/j.clema.2022.100056>
- Todkar, B. S., Deorukhkar, O. A., & Deshmukh, S. M. (2016). Extraction of silica from rice husk. *International Journal of Engineering Research*, 12(3), 69–74.
- Wahid, H. A., Ramli, M. A., Razak, M. I. A., & Zulkepli, M. I. S. (2018). Determination of zakat recipient to flood victims. *International Journal of Academic Research in Business and Social Sciences*, 7(12), 1289–1304. <https://doi.org/10.6007/IJARBS/v7-i12/3767>
- Wang, Z., Wang, H., Zhang, T., & Xu, C. (2017). Investigation on absorption performance between cement and emulsified asphalt with UV-Vis spectrophotometer. *Construction and Building Materials*, 136, 256–264. <https://doi.org/10.1016/j.conbuildmat.2017.01.016>
- Wang, D., Shi, C., Farzadnia, N., Shi, Z., & Jia, H. (2018). A review on effects of limestone powder on the properties of concrete. *Construction and Building Materials*, 192, 153–166. <https://doi.org/10.1016/j.conbuildmat.2018.10.119>
- Yadollahi, M. M., Benli, A., & Demirboğa, R. (2015). The effects of silica modulus and aging on compressive strength of pumice-based geopolymer composites. *Construction and Building Materials*, 94, 767–774. <https://doi.org/10.1016/j.conbuildmat.2015.07.052>
- Yang, X., Zhu, W., & Yang, Q. (2008). The viscosity properties of sodium silicate solutions. *Journal of Solution Chemistry*, 37, 73–83. <https://doi.org/10.1007/s10953-007-9214-6>
- Yazdani, S., & Singh, A. (2013). *New developments in structural engineering and construction*. Research Publishing Services.
- Zabihi-Samani, M., Mokhtari, S. P., & Raji, F. (2018). Effects of fly ash on mechanical properties of concrete. *Journal of Applied Engineering Sciences*, 8(2), 35–40. <https://doi.org/10.2478/jaes-2018-0016>